

FSAG: Enhancing Human-to-Dexterous-Hand Finger-Specific Affordance Grounding via Diffusion Models

Yifan Han^{1,2}, Pengfei Yi^{1,2}, Junyan Li^{1,2}, Hanqing Wang³, Gaojing Zhang⁴, Qi Peng Liu⁵, Wenzhao Lian^{5†}



Fig. 1. **Overview.** FSAG learns finger-specific affordance fields from human demonstrations by leveraging hand–object interaction semantic priors from a frozen Stable Diffusion [1]. The predicted per-finger contact maps are fused with depth/segmentation to project contacts onto 3D geometry and drive an approach–closure–hold motion planner. Requiring no robot action data, FSAG yields functional, stable grasps on everyday objects and tools and transfer across dexterous-hand embodiments.

Abstract—Dexterous grasp synthesis remains a central challenge: the high dimensionality and kinematic diversity of multi-fingered hands prevent direct transfer of algorithms developed for parallel-jaw grippers. Existing approaches typically depend on large, hardware-specific grasp datasets collected in simulation or through costly real-world trials, hindering scalability as new dexterous hand designs emerge. To this end, we propose a data-efficient framework, which is designed to bypass robot grasp data collection by exploiting the rich, object-centric semantic priors latent in pretrained generative diffusion models. Temporally aligned and fine-grained grasp affordances are extracted from raw human video demonstrations and fused with 3D scene geometry from depth images to infer semantically grounded contact targets. A kinematics-aware retargeting module then maps these affordance representations to diverse dexterous hands without per-hand retraining. The resulting system produces stable, functionally appropriate multi-contact grasps that remain reliably successful across common objects and tools, while exhibiting strong generalization across previously unseen object instances within a category, pose variations, and multiple hand embodiments. This work (i) introduces a semantic affordance extraction pipeline leveraging vision–language generative priors for dexterous grasping, (ii) demonstrates cross-hand generalization without constructing hardware-specific grasp datasets, and (iii) establishes that a single depth modality suffices for high-performance grasp synthesis when coupled with foundation-model semantics. Our results highlight a path toward scalable, hardware-agnostic dexterous manipulation driven by human demonstrations and pretrained generative models.

I. INTRODUCTION

Reliable grasp synthesis remains a central, yet unresolved, challenge in dexterous robot manipulation. Compared with parallel-jaw grippers, multi-fingered dexterous hands offer

substantially higher kinematic expressivity and potential contact richness, but this increase in dimensionality and hand–object–environment interaction complexity dramatically amplifies the difficulty of learning and deploying robust grasp strategies. The classical problem can be informally factorized into (i) “*how to grasp*”: the structured, role-aware coordination of fingers, contacts, approach direction, and hand synergies, and (ii) “*where to grasp*”: the spatial localization of functionally exploitable object regions. Despite rapid progress, existing methods typically address these two issues in isolation, leading to brittle policies, embodiment entanglement, and limited cross-object generalization.

On “*how to grasp*”, recent works leverage reinforcement learning or large-scale supervised training in simulation to explore expansive action spaces [2], [3]. However, simulation-trained policies customarily rely on privileged, complete, and noise-free geometric states, which are rarely attainable in real-world deployments. This induces significant sim-to-real gaps when facing realistic sensing artifacts such as partial views, self-occlusions, depth discontinuities, and modality noise. An alternative line—direct large-scale real-world data collection (e.g., AnyDexGrasp [4])—suffers from prohibitive operational cost and still struggles to generalize to unseen dexterous hand embodiments. A core culprit is representational overfitting: action/policy parameterizations are tightly coupled to a specific hand model’s joint layout, contact affordances, and actuation limits, precluding systematic transfer.

On “*where to grasp*”, prevailing affordance research yields coarse region-of-interest predictions [5], [6]. While such representations offer a spatial prior for potential contact regions, they stop short of encoding the per-finger engagement strategy and the geometry-conditioned sequencing necessary for stable multi-contact closure. Thus, although they identify candidate regions, they fail to specify the fine-grained per-finger instructions required for dexterous manipulation (e.g.,

¹Institute of Automation, Chinese Academy of Sciences.; ²School of Artificial Intelligence, University of Chinese Academy of Sciences.;

³The Hong Kong University of Science and Technology (Guangzhou);

⁴University of Sussex.; ⁵School of Artificial Intelligence, Shanghai Jiao Tong University. lianwenzhao@sjtu.edu.cn.;

†Corresponding Author.

contact assignments, approach vectors, and local-geometry adaptations). Recasting contact reasoning as keypoint detection is likewise insufficient: reliable contact loci often lack discriminative RGB cues and hinge on object-part semantics and inter-finger relations that appearance-only backbones (e.g., CNNs/ViTs [7]) do not capture.

Our core idea to tackle the above challenges is that Internet-scale text-to-image diffusion models internalize multi-level knowledge about objects, parts, materials, and functional geometry [1]. Prior work [8] shows that intermediate denoising features encode exactly the semantic priors missing in standard discriminative backbones, and that these features can be repurposed—not to generate data, but to ground grasp semantics.

Building on this insight, we propose to infer a *Finger-Specific Affordance Field (FSAF)* that unifies the “how” and “where”: a dense, object-conditioned mapping that assigns, for each prospective surface location, structured likelihoods and role descriptors for individual fingers, jointly capturing feasible contact placement, approach direction hypotheses, and inter-finger relational compatibility. Specifically, we repurpose a frozen Stable Diffusion[1] U-Net as a semantic backbone to infer a FSAF and couple it with a kinematics-aware planner for on-table execution. Once FSAF is inferred, we compose novel grasps without additional tele-operation and transfer across heterogeneous dexterous hands via object-centric planning. This affordance-based representation enables more precise manipulation from only a small number of human demonstrations and supports deploying a single policy across multiple dexterous hands. Experiments demonstrate state-of-the-art performance on seen and unseen objects—superior affordance grounding and a 90% grasp success rate—with cross-embodiment transfer to different dexterous hands. In summary, we make the following contributions:

- **Finger-Specific Affordance Field (FSAF).** We introduce a fine-grained, per-finger affordance representation that leverages vision–language generative priors to jointly encode object affordance functions and contact-level manipulation semantics, decomposing monolithic grasp poses into semantically grounded finger role assignments.
- **Demonstration-light, affordance-conditioned grasp synthesis.** Our grasp generation consumes the inferred FSAF to synthesize stable, role-constrained multi-finger grasp configurations without requiring large-scale tele-operation demonstration corpora, substantially reducing data collection burden.
- **Cross-embodiment generalization.** We achieve direct transfer of grasp strategies across heterogeneous dexterous hands, evidencing that the proposed affordance abstraction disentangles grasp semantics from specific embodiment kinematics.

II. RELATED WORK

A. Learning from Human Demonstration Videos

Learning from human demonstration videos is central to robot learning because such data are easier to collect and encode strong task priors [6], [9]; however, a persistent embodiment gap separates human hands from robotic dexterous end-effectors. The prevailing remedy is retargeting—mapping human motions to robot kinematics [10], [11], [12]—which is effective for teleoperation and data gathering but typically still requires reinforcement learning in simulation to attain dexterous proficiency, thereby introducing a sim-to-real gap and limiting cross-embodiment generalization. Recently, a more fundamental route is to learn manipulation structure from human hand data that robots can directly consume. For parallel-jaw grippers, PointPolicy [13] uses video-derived keypoints to supervise gripper control; however, such position-only cues under-specify dexterous-hand interaction. In this work, we therefore learn finger-specific affordances from human demonstrations—object-conditioned descriptors that specify, per finger, contactable regions and approach directions over time—to represent how dexterous hands should interact with objects.

B. Object-centric Representation Learning

Much of object-centric grasping is tailored to parallel-jaw grippers, representing grasps by 2D/3D locations. Such position-only cues under-specify dexterous-hand interactions [14], [15]. In addition, a subset of dexterous hand approaches relies on template matching, built around exemplars specific to the object or the task, thus having limited generalizability to novel objects/tasks [16], [17]. Contact-centric representations improve task relevance but require complex pipelines and costly data collection to obtain dexterous-hand contact regions [18], [19]. More recently, interaction-driven approaches such as CMKA [20] learn interaction regions from web imagery, yet map object keypoints to wrist, index, and little-finger anchors, effectively producing a single grasp parameterized by three points and limiting performance to on-shelf settings. These limitations motivate per-finger contact representations rather than region- or point-only cues. We learn per-finger contact cues and, via depth-and-segmentation projection, map them onto object surfaces, to further derive precise tabletop grasps.

C. Affordance Learning

The concept of affordance was popularized by psychologist James Gibson [21], which aims to highlight the actionable areas on objects, is crucial for robotic grasping and manipulation in dynamic, complex, and physical environments. Previous research has achieved remarkable progress in learning affordance knowledge from Human-Object-Interaction (HOI) images [22], [23] and videos [24], [5], language instructions [25], and 3D point clouds [26], [27]. More recently, researchers have expanded the reasoning ability of multimodal large language models into affordance learning [28], [29], achieving advanced affordance

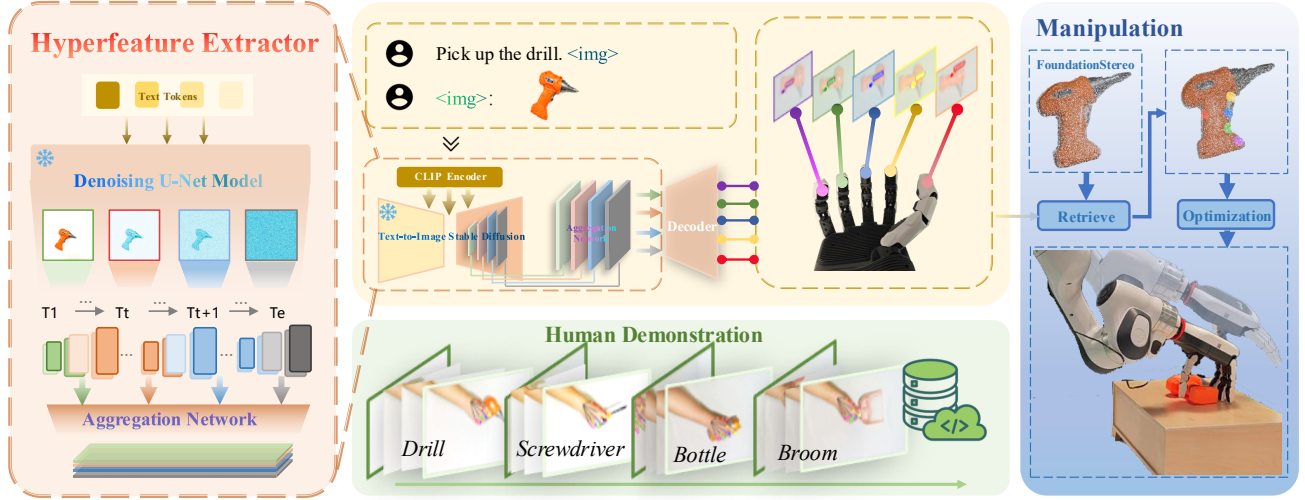


Fig. 2: **Pipeline overview.** (1) *Hyperfeature extraction*: A frozen text-to-image diffusion U-Net encodes the object image with text conditioning. Multi-timestep, multi-scale activations are aggregated into hyperfeatures A_g . (2) *Finger-specific affordance grounding*: An FPN-style decoder maps A_g to five per-finger likelihood maps \hat{H} supervised by fingertip labels from human demonstrations. (3) *Manipulation*: Back-projecting GroundingDINO-SAM2 masks with FoundationStereo depth yields a partial object point cloud; peaks of \hat{H} are lifted to 3D and local normals define phase-labeled waypoints (*approach*, *closure*, *hold*). A damped least-squares QP tracks these waypoints under joint and collision constraints to execute dexterous grasps.

reasoning and generalization abilities. Moreover, the text-to-image diffusion model [1] shows promising affordance-aware understanding ability by generating precise hand-object images [8]. However, most approaches localize coarse object regions (e.g., boxes or masks), which is insufficient for fine-grained, finger-specific guidance required by dexterous hands—motivating representations at the per-finger contact level.

III. METHODS

We present a perception-to-optimization framework that learns *finger-specific affordances* from human demonstrations and converts them into executable dexterous grasps, as shown in Fig. 2. Semantically grounded hyperfeatures from a frozen text-to-image diffusion model [1] are decoded into five-channel per-finger likelihood maps, which guide contact selection on a reconstructed object point cloud. Local surface geometry defines waypointed approach/closure trajectories that are tracked via a damped least-squares QP under joint and collision constraints. As grasp execution is optimization-based, the pipeline transfers across dexterous hands with little or no retraining.

A. Data Collection

We construct a finger-wise contact affordance dataset from human demonstration videos using a custom data acquisition pipeline. For each recorded grasp sequence, we first automatically detect 2D hand keypoints with the RTMPose [30] hand pose estimator. We then identify (i) an *object-only* keyframe in which the target object is fully visible and no hand pixels are present, and (ii) the earliest *stable* grasp frame in which the human hand establishes clear contact with the object.

This pair of frames form one training sample: the object-only frame provides a clean visual context of the object’s geometry and texture, while the grasp frame provides the supervisory signal for finger-specific contact localization.

On the image lattice $\Omega = \{0, \dots, h-1\} \times \{0, \dots, w-1\}$, each fingertip k with center μ_k induces a Gaussian channel $H_k(u) = \exp(-\|u - \mu_k\|_2^2 / (2\sigma^2))$ for $u \in \Omega$; stacking yields a tensor H of shape $5 \times h \times w$. We set $\sigma = \min(h, w)/64$ and train the predictor \hat{H} to regress H using MSE.

B. Finger-Specific Affordance Representation from Diffusion Models

1) *Feature synthesis and hyperfeature aggregation*: Empirical evidence that diffusion models generate precise hand-object grasp [8] scenarios indicates that Stable Diffusion [1] has already acquired the grasp-critical feature space, integrating holistic affordance semantics with nuanced image details via its generative learning process. Inspired by prior work [8], [31], we leverage the rich semantic grounding capability of large pretrained text-to-image diffusion models to localize finger-specific contact affordances on object images. Distinct from previous approaches, we jointly harvest both visual and textual affordance semantics from Stable Diffusion. Roughly speaking, we employ a U-Net backbone comprising convolutional blocks, downsampling / upsampling paths, skip connections, and cross-attention modules. At each denoising timestep, cross-attention injects textual embeddings into the visual feature stream, encouraging intermediate activations to align with interpretable semantic concepts. Specifically, given an image-text pair (x_0, s) , we encode a latent $z_0 = E(x_0)$ with the variational autoencoder (VAE) and follow the standard *latent* forward

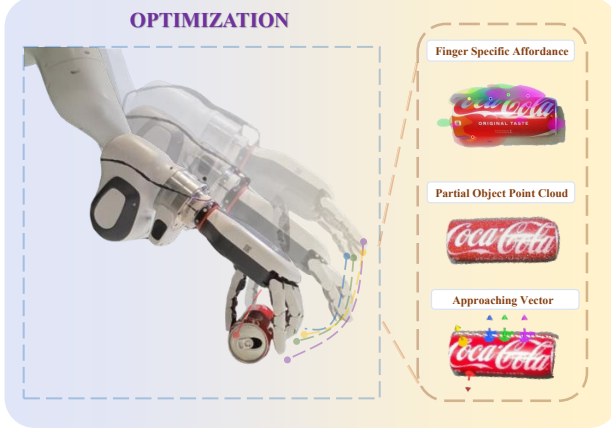


Fig. 3: **Right:** (1) finger-specific affordance likelihoods predicted from diffusion-derived hyperfeatures; (2) partial object point cloud reconstructed by back-projecting GroundingDINO-SAM2 segmentation with FoundationStereo depth; (3) approach vectors obtained from local surface normals around the selected contact candidates. **Left:** a damped least-squares QP tracks phase-labeled waypoints to execute a dexterous grasp.

noising process

$$z_t = \sqrt{\bar{\alpha}_t} z_0 + \sqrt{1 - \bar{\alpha}_t} \varepsilon, \quad \varepsilon \sim \mathcal{N}(0, I), \quad (1)$$

where $\bar{\alpha}_t = \prod_{\tau=1}^t \alpha_\tau$ as defined in [1]. We keep the text encoder $T(\cdot)$ frozen and obtain token embeddings $c = T(s)$. For computational reasons, we run the diffusion network for T timesteps but only select a subset \mathcal{S} with $|\mathcal{S}| = S$ for feature aggregation. Feeding (z_t, t, c) into a frozen diffusion U-Net yields multi-scale activations:

$$\{A_{v,1}^{(t)}, A_{v,2}^{(t)}, \dots, A_{v,L}^{(t)}\}, \quad t \in \mathcal{S},$$

Here, $A_{v,\ell}^{(t)} \in \mathbb{R}^{B \times C_\ell \times H_\ell \times W_\ell}$ denotes the feature map from the ℓ -th U-Net block at timestep t .

To summarize complementary semantics across scales and timesteps, we attach lightweight bottlenecks $\{b_\ell\}_{\ell=1}^L$ (shared across timesteps) and learn mixing coefficients $\{w_{\ell,t}\}_{\ell=1, t \in \mathcal{S}}^L$ to produce a global affordance descriptor:

$$A_g = \sum_{t \in \mathcal{S}} \sum_{\ell=1}^L w_{\ell,t} b_\ell\left(A_{v,\ell}^{(t)}\right). \quad (2)$$

In practice, each b_ℓ is a 1×1 convolution followed by global average pooling to a fixed d -dimensional vector. We parameterize $\tilde{w}_{\ell,t}$ freely and apply a softmax over all (ℓ, t) .

2) Finger-Specific Affordance Heatmap Prediction: To enhance the fine-grained finger-specific affordance grounding ability while preserving high-level semantic discrimination and recovering spatial details, we proposed a feature pyramid network (FPN)-style decoder, which progressively upsamples A_g while injecting lateral features from shallower resolutions, producing a dense fused feature map suitable for contact prediction.

Given the dense hyperfeature $A_g \in \mathbb{R}^{B \times C \times h \times w}$, we decode it with three lateral 1×1 projections $\{\phi_r\}_{r=3}^1$ (to channels

$c_r \in \{256, 128, 64\}$) and a top-down pathway. Let target sizes $s_3 = (h, w)$, $s_2 = (2h, 2w)$, $s_1 = (H_{out}, W_{out})$, U_s be bilinear upsampling to size s , τ_r a 1×1 adapter, and ψ_r a 3×3 smoothing conv with nonlinearity. With $F_4 \equiv 0$, we compute

$$F_r = \psi_r\left(U_{s_r}(\tau_r(F_{r+1})) + U_{s_r}(\phi_r(A_g))\right), \quad r = 3, 2, 1, \quad (3)$$

and obtain the per-finger heatmaps by a final 3×3 projection

$$\hat{H} = \kappa(F_1) \in \mathbb{R}^{B \times K \times H_{out} \times W_{out}}, \quad K = 5. \quad (4)$$

We optimize a mean squared error (MSE) loss over all fingers and pixels:

$$\mathcal{L}_{\text{MSE}} = \frac{1}{5|\Omega|} \sum_{k=1}^5 \sum_{u \in \Omega} (\hat{H}_k(u) - H_k(u))^2. \quad (5)$$

C. Finger-Specific Affordance Matching for Grasp Planning

Upon obtaining the finger-specific affordances, we employ a perception-to-optimization pipeline (Fig. 3) to synthesize executable dexterous grasp motions. We deliberately eschew any learned policy so that the method can be ported across distinct dexterous hand embodiments without model modification or retraining; adopting a pure motion-planning and optimization formulation preserves cross-embodiment generality. Our perception pipeline reconstructs a partial object point cloud by first generating a dense depth map from stereo infrared (IR) using the FoundationStereo [32]. The target object mask, segmented by GroundingDINO-SAM2 [33], [34], is then back-projected using camera intrinsics to yield the final 3D point cloud. Using the finger keypoints obtained in Section III-B, we first re-project the entire 3D point cloud onto the image plane. Then, for each finger keypoint, we use the previously described method to select the N point-cloud projections that are closest to it in the image, forming robust fingertip contact candidates.

Approach Vector Construction: Given the predicted per-finger contact locations c_k , we estimate a consistent surface normal \hat{n}_k by fitting a local tangent plane to the object point cloud and resolving its orientation with an object-centric rule (normal oriented toward the contact patch). We then parameterize a short, geometry-aligned 1D approach vector for each finger:

$$\gamma_k(s) = c_k + s \hat{n}_k, \quad s \in \mathbb{R}, \quad (6)$$

and instantiate three phase anchors along this curve: *approach* ($s > 0$), *closure* ($s \rightarrow 0^+$), and *hold* ($s < 0$, introducing a small preload). For each phase $w \in \{\text{app}, \text{clo}, \text{hold}\}$, the Cartesian target is defined as $p_k^*(w) = \gamma_k(s_w)$. A hand-level waypoint is obtained by taking the barycentric average over all finger targets.

Task Formulation: Let $q \in \mathbb{R}^{n_q}$ be the full arm-hand joint vector. For fingertip pad $k \in \{1, \dots, K\}$, let $p_k(q) \in \mathbb{R}^3$ be its forward kinematics and $J_k(q) = \partial p_k / \partial q \in \mathbb{R}^{3 \times n_q}$ its Jacobian. The goal is to drive all fingertip pads to the waypoint positions $\{p_k^*(w)\}$. At control step t with active waypoint w_t , define the per-fingertip tracking residuals $r_k(q_t) = p_k(q_t) - p_k^*(w_t)$. Additionally, we model finger underactuation via

a coupling residual $e_c(q_t)$ with Jacobian $J_c(q_t)$, which is penalized in the objective (soft constraint):

$$r_t = \begin{bmatrix} r_1(q_t) \\ \vdots \\ r_K(q_t) \\ r_{\text{coup}}(q_t) \end{bmatrix} = \begin{bmatrix} p_1(q_t) - p_1^*(w_t) \\ \vdots \\ p_K(q_t) - p_K^*(w_t) \\ e_c(q_t) \end{bmatrix}, \quad J_t = \begin{bmatrix} J_1(q_t) \\ \vdots \\ J_K(q_t) \\ J_c(q_t) \end{bmatrix},$$

with weight matrix $W = \text{diag}(\omega_1 I_3, \dots, \omega_K I_3, \lambda_{\text{coup}} I_{m_c})$.

A Gauss–Newton step solves for Δq_t via the convex quadratic program:

$$\begin{aligned} \min_{\Delta q_t} \frac{1}{2} \|W^{1/2}(J_t \Delta q_t + r_t)\|_2^2 + \frac{\lambda_{\text{damp}}}{2} \|\Delta q_t\|_2^2 \\ \text{s.t. } q_{\min} - q_t \leq \Delta q_t \leq q_{\max} - q_t \\ G_{\text{col}} \Delta q_t \leq h_{\text{col}} \end{aligned} \quad (7)$$

where λ_{damp} is a Levenberg–Marquardt damping term; the first constraint enforces joint bounds and the second specifies linearized collision avoidance constraints (including table contact and self-collisions). We warm-start OSQP [35] at q_t , set $q_{t+1} = q_t + \Delta q_t^*$, and recompute forward kinematics for the next step, ensuring motion continuity and avoiding commands that would place the robot in unreachable configurations.

Execution. The controller is implemented in the Mink framework [36]; solutions are computed in simulation and synchronized to the physical robot in real time.

IV. EXPERIMENTS

In this section, we conduct comprehensive experiments to validate our method from three complementary perspectives:

RQ1: Does the proposed finger-specific grasp representation outperform prior keypoint/affordance grounding, and does leveraging vision–language priors from Stable Diffusion model yield gains over discriminative backbones?

RQ2: Does the method improve the functional correctness and stability of dexterous grasps on seen and unseen objects, even for objects with weak part cues?

RQ3: Does the learned finger-specific affordance representation transfer across dexterous hands with minimal adaptation?

A. Experimental Setup

Dataset: We collect 130 *finger-specific* human grasp demonstrations over 13 everyday objects (10 per object; e.g., banana, screwdriver, bottle). For evaluation, we test on seven *unseen* objects that include both (i) new instances of previously seen categories and (ii) entirely novel categories (e.g., wrench, hammer).

Implementation Details: We train for 4,000 steps with batch size 2 on a single NVIDIA H100 GPU using AdamW (initial learning rate 10^{-3} with cosine decay). Raw RGB frames are resized to 640×320 with letterboxing when necessary to preserve aspect ratio, and pixel intensities are normalized to $[0, 1]$. Predicted and ground-truth finger heatmaps are uniformly rescaled to 448×448 following

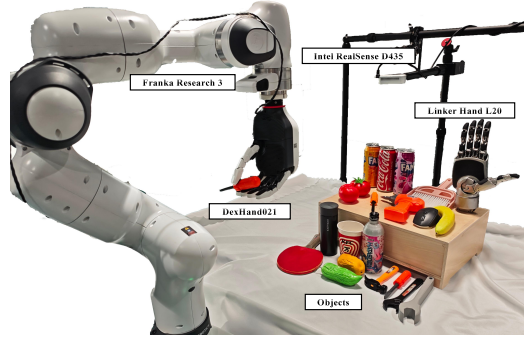


Fig. 4: Robotic arm and dexterous-hand experimental platform used in our study.

saliency-grounding conventions, and each per-finger heatmap is re-normalized to integrate to 1. All results are averaged over 3 random seeds. The robotic arm–dexterous-hand platform is shown in Fig. 4; the real-world setup comprises two dexterous hands (DexHand021 and Linker Hand L20), a Franka arm, and a RealSense 435 camera.

Evaluation Metrics: For finger-specific affordance grounding, We report KLD, SIM, and NSS [37]:

- **KLD** (lower is better): Kullback–Leibler divergence between predicted and ground-truth heatmaps.
- **SIM** (higher is better): Normalized histogram intersection (similarity).
- **NSS** (higher is better): Normalized Scanpath Saliency; per finger we sample the annotated keypoint location as a fixation.

For Dexterous functional grasping, we follow the definitions of metrics provided in [4] and [5]: **Grasping Success Rate (Suc. R.)**: A grasp is considered successful if the object can be lifted above 0.1 m and held stable longer than 3 seconds. Here, grasping specifically refers to grasping based on manipulation affordances.

B. Results of Finger-Specific Affordance Grounding

Because there is no prior work that directly couples vision–language models with fine-grained, finger-specific affordance keypoints, we select two closest approaches as baselines. (1) Rekep [38] is a robotic manipulation keypoint prediction framework that extracts image features using DINO and obtains keypoints via unsupervised clustering. (2) CMKA [20] leverages exocentric (third-person) interaction images as input, applies SAM [39] for multi-scale object segmentation, and then performs clustering over the segmentation-driven feature hierarchy to learn object affordance keypoints. To ensure fairness, we train CMKA [20] using the exocentric interaction images from our dataset, keeping all other hyperparameters unchanged. For metric computation, we follow a procedure consistent with CMKA: the predicted keypoints are first rescaled to the original image resolution, then converted into heatmaps by placing Gaussian kernels (with σ set to shorter side of image size / 64) centered at each keypoint. To validate the necessity of large-scale generative models in our framework, we conduct ablations

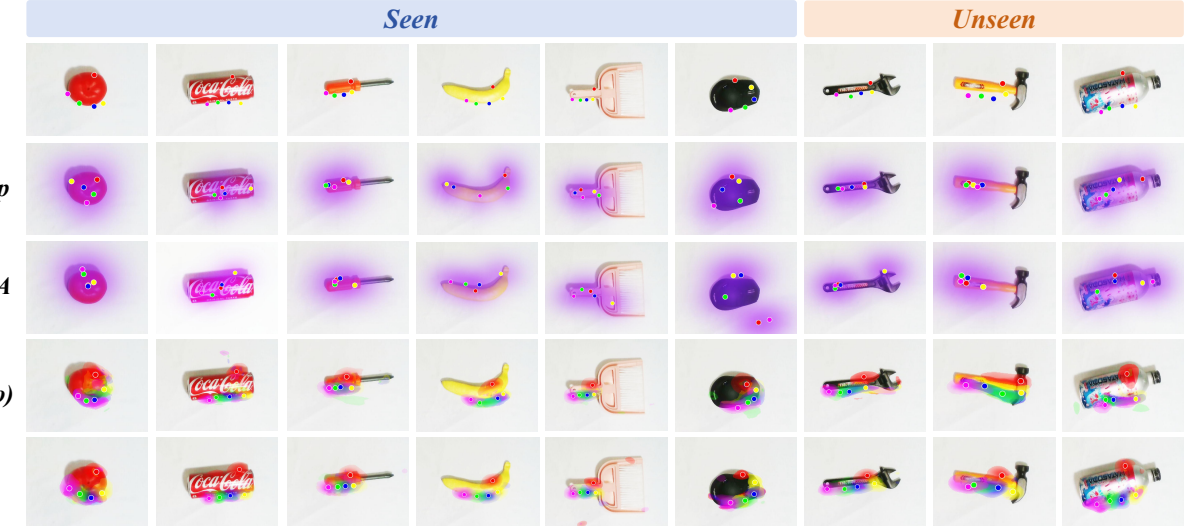


Fig. 5: **Qualitative comparison of finger-specific affordance grounding.** Left: *Seen* objects; Right: *Unseen* objects. Rows show ReKep, CMKA, Ours (DINO features), and Ours (Stable Diffusion). Overlays visualize five per-finger likelihood maps; colored dots indicate annotated fingertip contacts. The diffusion-based variant produces sharper, finger-disentangled hotspots aligned with functional parts and preserves localization quality on unseen tools. ReKep and CMKA each produce keypoints directly and a single-channel heatmap is generated via post-processing following CMKA, thus their overlays are rendered in a single purple color, whereas our method outputs five-channel heatmaps rendered with five distinct colors.

TABLE I: Comparison and ablation on the finger-specific affordance grounding benchmark. Best results in **bold**. (\uparrow / \downarrow denote higher/lower is better.)

Model / Variant	KLD(\downarrow)	SIM(\uparrow)	NSS(\uparrow)
ReKep [38]	10.127	0.173	1.801
CMKA [20]	11.184	0.177	1.861
Ours (CLIP)	6.690	0.355	3.815
Ours (DINO)	3.301	0.473	5.016
Ours (SD)	2.491	0.551	5.518

that replace the diffusion-derived hyperfeatures with discriminative backbones CLIP [40] and DINO [41] used purely as feature extractors.

Table I shows that both ReKep and CMKA fall short on finger-specific affordance grounding: ReKep’s unsupervised keypoints, learned purely from image features, lack the semantic selectivity needed to localize functionally meaningful, finger-wise contacts, while CMKA’s segmentation-driven hierarchy struggles when objects do not present distinctive, part-aligned regions. Fig. 5 (left, *seen*) and (right, *unseen*) qualitatively reveal these failure cases where on objects with weak or uniform appearance cue, e.g., the smooth, texture-poor *tomato* and the monochrome *mouse*, both baselines produce diffuse, centroid-biased blobs and scattered contact dots that either bleed across boundaries or miss functional parts. Our model simultaneously improves all three metrics—lower KLD and higher SIM/NSS—indicating more precise localization of affordance-relevant regions rather than generic centers or silhouette edges.

Holding data, labels, losses, and training schedule fixed

while varying only the feature extractor, we isolate the contribution of diffusion-derived hyperfeatures. **KLD** increases by $1.33\times$ compared with DINO and $2.69\times$ with CLIP, while **SIM** drops by 14.2%/35.6% and **NSS** by 9.1%/30.9%. Ours (DINO) tends to merge adjacent fingers into single peaks and produces broader activations with boundary spill-over. Besides, on *unseen* elongated tools (e.g., *hammer*), it allocates excess activation to the visually salient head rather than the grasp-functional handle. In contrast, our diffusion-based model maintains sharp, part-aligned peaks along the handle and places stabilizing secondary contacts on supporting faces. Across both seen and unseen items (e.g., *screwdriver*, *wrench*, *bottle*), diffusion hyperfeatures consistently suppress three dominant errors, i.e., centroid collapse, boundary spill-over, and fingertip swapping, supporting **RQ1** that diffusion-derived hyperfeatures are critical for precise per-finger affordance localization.

C. Functional Affordance Grasping with High-DOF Hands

Our evaluation targets *on-table*, affordance-driven dexterous grasping with finger-specific contacts and human-consistent grasp sites. Existing simulation-trained policies [2] optimize for success in simplified settings and cannot select grasp sites following human conventions (e.g., grasping a hammer by its head). To assess alignment with human grasp choices within our setting, we include two point-cloud-based imitation learning policies (Diffusion Policy 3D [42] and ACT-3D [43]) trained from our teleoperated demonstrations(30 trajectories). We also compare to CMKA representing a recent affordance-based dexterous grasping approach. We evaluate CMKA strictly under its original, unmodified pipeline: we directly use the three keypoints predicted by CMKA, lift them to 3D, assign them to the

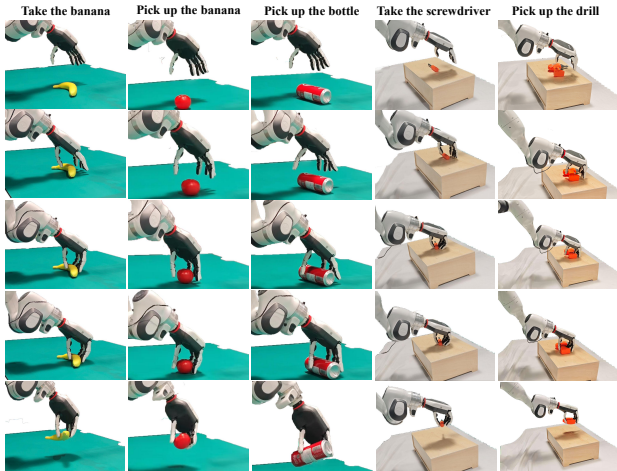


Fig. 6: **Affordance-driven dexterous grasping in the real world.** Representative rollouts on everyday objects and tools; columns denote tasks (banana, bottle, tomato, screwdriver, drill).

TABLE II: Performance comparison across different methods on common objects and tools manipulation tasks. Each cell reports $N=20$ trials per object (S = seen, U = unseen).

Model	Common Objects (%)			Tools (%)	
	Bottle (S/U)	Banana	Tomato	Screwdriver	Drill
ACT-3D [43]	30/25	30	50	30	40
Diffusion Policy 3D [42]	40/40	50	45	0	30
CMKA [20]	30/20	20	0	0	60
Ours	100/85	85	90	60	70

functional finger, little finger, and wrist, and then execute the method’s fixed grasp execution strategy.

As shown in Tab. II, the conventional imitation-learning baselines tend to reproduce trajectories close to demonstrations: as object morphology varies, they do not proactively adapt their strategy, leading to significantly degraded performance both on seen objects with poses absent from the training data and on unseen objects. CMKA’s performance is limited by the layered segmentation output of SAM; as discussed in Section II-B, for objects that lack salient part delineation such as tomatoes and bananas, it often fails to predict correct grasp locations. Moreover, because it executes a preprogrammed grasp approaching motion, the fingers collide with the table surface when attempting to grasp low-profile objects such as bananas and screwdrivers, thus preventing successful task completion. By contrast, our method achieves higher success on common objects and remains robust on previously unseen instances within the same categories. In Fig. 6, per-finger affordance inference places contacts on grasp-functional geometry, while robust stereo depth estimation provides stable surface normals for accurate on-table execution. The geometry-aligned *Approach Vector* co-optimizes wrist pose and finger trajectories relative to the tabletop object, producing table-skimming entries that reliably avoid finger-table collisions, particularly beneficial for low-profile objects.

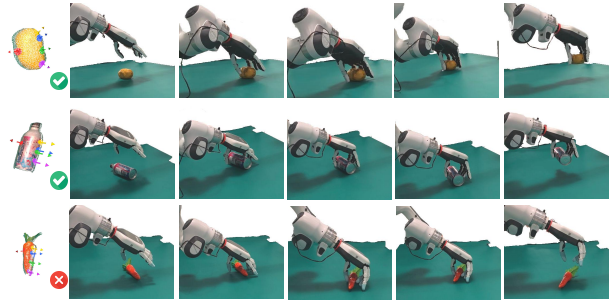


Fig. 7: Zero-shot generalization on unseen objects

TABLE III: Grasp success rates across different hand embodiments.

Model	Common Objects (%)			Tools (%)	
	Bottle (S/U)	Banana	Tomato	Screwdriver	Drill
DexHand021	100/85	85	90	60	70
Linker Hand L20	100/80	90	100	70	90

D. Cross-Embodiment Evaluation

As shown in the right column of Fig. 1, we maintain the same perception-to-optimization pipeline across dexterous-hand embodiments, performing finger-specific affordance inference fused with depth, followed by an approach–closure–hold planner. We transfer the pipeline from DexHand021 (12+5 DOFs) to Linker Hand L20 (16+5 DOFs) via kinematic retargeting of fingertip targets; perception and affordance inference remain unchanged. As shown in Tab. III, grasp success remains statistically unchanged across embodiments. This invariance indicates that the proposed finger-specific affordance representation and geometry-aligned waypoint construction decouple grasp semantics from hand morphology, enabling deployment without hand-specific re-training.

V. CONCLUSION AND FUTURE WORK

We leverage pretrained generative models’ understanding of hand–object interactions to extract both high-level object semantics and fine-grained visual cues, and fuse these with a small set of human demonstrations providing fingertip annotations. This enables learning *finger-specific affordances* that unify perception and control: our representation captures not only *where* to act but also *how* to act. Built on this, our FSAG-based motion planning maps dexterous-hand postures onto finger-specific contacts, yielding stable functional grasps and generalization across multiple dexterous-hand embodiments. Empirically, our approach substantially outperforms contemporary methods on both affordance localization accuracy and functional grasping success rate.

As illustrated in Fig. 7, occasional failures on slender objects arise primarily from the execution: a simple, fixed-offset open-loop closure can induce rotation or slip even when contact targets are valid. Next, we will close the loop around FSAF contacts via learned residual-impedance/operational-

space control with contact-force estimation and slip detection, yielding more robust and dynamic manipulation.

REFERENCES

- [1] R. Rombach, A. Blattmann, D. Lorenz, P. Esser, and B. Ommer, “High-resolution image synthesis with latent diffusion models,” in *Proceedings of the IEEE/CVF conference on computer vision and pattern recognition*, 2022, pp. 10 684–10 695.
- [2] Y. Xu, W. Wan, J. Zhang, H. Liu, Z. Shan, H. Shen, R. Wang, H. Geng, Y. Weng, J. Chen *et al.*, “Unidexgrasp: Universal robotic dexterous grasping via learning diverse proposal generation and goal-conditioned policy,” in *Proceedings of the IEEE/CVF Conference on Computer Vision and Pattern Recognition*, 2023, pp. 4737–4746.
- [3] R. Wang, J. Zhang, J. Chen, Y. Xu, P. Li, T. Liu, and H. Wang, “Dexgraspnet: A large-scale robotic dexterous grasp dataset for general objects based on simulation,” *arXiv preprint arXiv:2210.02697*, 2022.
- [4] H.-S. Fang, H. Yan, Z. Tang, H. Fang, C. Wang, and C. Lu, “Anydex-grasp: General dexterous grasping for different hands with human-level learning efficiency,” *arXiv preprint arXiv:2502.16420*, 2025.
- [5] H. Luo, W. Zhai, J. Zhang, Y. Cao, and D. Tao, “Learning visual affordance grounding from demonstration videos,” *IEEE Transactions on Neural Networks and Learning Systems*, 2023.
- [6] ———, “Learning affordance grounding from exocentric images,” in *Proceedings of the IEEE/CVF conference on computer vision and pattern recognition*, 2022, pp. 2252–2261.
- [7] A. Dosovitskiy, L. Beyer, A. Kolesnikov, D. Weissenborn, X. Zhai, T. Unterthiner, M. Dehghani, M. Minderer, G. Heigold, S. Gelly, J. Uszkoreit, and N. Houlsby, “An image is worth 16x16 words: Transformers for image recognition at scale,” in *International Conference on Learning Representations*, 2021. [Online]. Available: <https://openreview.net/forum?id=YicbFdNTTy>
- [8] J. Yang, B. Li, F. Yang, A. Zeng, L. Zhang, and R. Zhang, “Boosting human-object interaction detection with text-to-image diffusion model,” *arXiv preprint arXiv:2305.12252*, 2023.
- [9] J. Ren, P. Sundaresan, D. Sadigh, S. Choudhury, and J. Bohg, “Motion tracks: A unified representation for human-robot transfer in few-shot imitation learning,” *arXiv preprint arXiv:2501.06994*, 2025.
- [10] Y. Qin, Y.-H. Wu, S. Liu, H. Jiang, R. Yang, Y. Fu, and X. Wang, “Dexmv: Imitation learning for dexterous manipulation from human videos,” in *European Conference on Computer Vision*. Springer, 2022, pp. 570–587.
- [11] S. Zhao, X. Zhu, Y. Chen, C. Li, X. Zhang, M. Ding, and M. Tomizuka, “Dexh2r: Task-oriented dexterous manipulation from human to robots,” *arXiv preprint arXiv:2411.04428*, 2024.
- [12] K. Li, P. Li, T. Liu, Y. Li, and S. Huang, “Maniptrans: Efficient dexterous bimanual manipulation transfer via residual learning,” in *Proceedings of the Computer Vision and Pattern Recognition Conference*, 2025, pp. 6991–7003.
- [13] S. Haldar and L. Pinto, “Point policy: Unifying observations and actions with key points for robot manipulation,” *arXiv preprint arXiv:2502.20391*, 2025.
- [14] M. K. Srirama, S. Dasari, S. Bahl, and A. Gupta, “Hrp: Human affordances for robotic pre-training,” *arXiv preprint arXiv:2407.18911*, 2024.
- [15] W. Dong, D. Huang, J. Liu, C. Tang, and H. Zhang, “Rtagrasp: Learning task-oriented grasping from human videos via retrieval, transfer, and alignment,” in *2025 IEEE International Conference on Robotics and Automation (ICRA)*. IEEE, 2025, pp. 1–7.
- [16] M. Kokic, D. Kragic, and J. Bohg, “Learning task-oriented grasping from human activity datasets,” *IEEE Robotics and Automation Letters*, vol. 5, no. 2, pp. 3352–3359, 2020.
- [17] C. Gabellieri, F. Angelini, V. Arapi, A. Palleschi, M. G. Catalano, G. Grioli, L. Pallottino, A. Bicchi, M. Bianchi, and M. Garabini, “Grasp it like a pro: Grasp of unknown objects with robotic hands based on skilled human expertise,” *IEEE Robotics and Automation Letters*, vol. 5, no. 2, pp. 2808–2815, 2020.
- [18] L. Yang, K. Li, X. Zhan, F. Wu, A. Xu, L. Liu, and C. Lu, “Oakink: A large-scale knowledge repository for understanding hand-object interaction,” in *Proceedings of the IEEE/CVF conference on computer vision and pattern recognition*, 2022, pp. 20 953–20 962.
- [19] Y.-W. Chao, W. Yang, Y. Xiang, P. Molchanov, A. Handa, J. Tremblay, Y. S. Narang, K. Van Wyk, U. Iqbal, S. Birchfield *et al.*, “Dexycb: A benchmark for capturing hand grasping of objects,” in *Proceedings of the IEEE/CVF conference on computer vision and pattern recognition*, 2021, pp. 9044–9053.
- [20] F. Yang, D. Luo, W. Chen, J. Lin, J. Cai, K. Yang, Z. Li, and Y. Wang, “Multi-keypoint affordance representation for functional dexterous grasping,” *arXiv preprint arXiv:2502.20018*, 2025.
- [21] J. J. Gibson, “The theory of affordances,” *Hilldale, USA*, vol. 1, no. 2, pp. 67–82, 1977.
- [22] Y. Yang, W. Zhai, H. Luo, Y. Cao, J. Luo, and Z.-J. Zha, “Grounding 3d object affordance from 2d interactions in images,” in *Proceedings of the IEEE/CVF International Conference on Computer Vision*, 2023, pp. 10 905–10 915.
- [23] Y. Shao, W. Zhai, Y. Yang, H. Luo, Y. Cao, and Z.-J. Zha, “Great: Geometry-intention collaborative inference for open-vocabulary 3d object affordance grounding,” *arXiv preprint arXiv:2411.19626*, 2024.
- [24] S. Bahl, R. Mendonca, L. Chen, U. Jain, and D. Pathak, “Affordances from human videos as a versatile representation for robotics,” in *Proceedings of the IEEE/CVF Conference on Computer Vision and Pattern Recognition*, 2023, pp. 13 778–13 790.
- [25] Y. Li, N. Zhao, J. Xiao, C. Feng, X. Wang, and T.-s. Chua, “Laso: Language-guided affordance segmentation on 3d object,” in *Proceedings of the IEEE/CVF Conference on Computer Vision and Pattern Recognition*, 2024, pp. 14 251–14 260.
- [26] S. Deng, X. Xu, C. Wu, K. Chen, and K. Jia, “3d affordancenet: A benchmark for visual object affordance understanding,” in *proceedings of the IEEE/CVF conference on computer vision and pattern recognition*, 2021, pp. 1778–1787.
- [27] A. Delitzas, A. Takmaz, F. Tombari, R. Sumner, M. Pollefeys, and F. Engelmann, “Scenefun3d: fine-grained functionality and affordance understanding in 3d scenes,” in *Proceedings of the IEEE/CVF Conference on Computer Vision and Pattern Recognition*, 2024, pp. 14 531–14 542.
- [28] H. Wang, S. Wang, Y. Zhong, Z. Yang, J. Wang, Z. Cui, J. Yuan, Y. Han, M. Liu, and Y. Ma, “Affordance-r1: Reinforcement learning for generalizable affordance reasoning in multimodal large language model,” *arXiv preprint arXiv:2508.06206*, 2025.
- [29] S. Qian, W. Chen, M. Bai, X. Zhou, Z. Tu, and L. E. Li, “Affordancemlm: Grounding affordance from vision language models,” in *Proceedings of the IEEE/CVF Conference on Computer Vision and Pattern Recognition*, 2024, pp. 7587–7597.
- [30] T. Jiang, P. Lu, L. Zhang, N. Ma, R. Han, C. Lyu, Y. Li, and K. Chen, “Rtmpose: Real-time multi-person pose estimation based on mmpose,” *CoRR*, 2023.
- [31] G. Luo, L. Dunlap, D. H. Park, A. Holynski, and T. Darrell, “Diffusion hyperfeatures: Searching through time and space for semantic correspondence,” *Advances in Neural Information Processing Systems*, vol. 36, pp. 47 500–47 510, 2023.
- [32] B. Wen, M. Trepte, J. Aribido, J. Kautz, O. Gallo, and S. Birchfield, “Foundationstereo: Zero-shot stereo matching,” in *Proceedings of the Computer Vision and Pattern Recognition Conference*, 2025, pp. 5249–5260.
- [33] S. Liu, Z. Zeng, T. Ren, F. Li, H. Zhang, J. Yang, Q. Jiang, C. Li, J. Yang, H. Su *et al.*, “Grounding dino: Marrying dino with grounded pre-training for open-set object detection,” in *European conference on computer vision*. Springer, 2024, pp. 38–55.
- [34] N. Ravi, V. Gabeur, Y.-T. Hu, R. Hu, C. Ryali, T. Ma, H. Khedr, R. Rädlé, C. Rolland, L. Gustafson, E. Mintun, J. Pan, K. V. Alwala, N. Carion, C.-Y. Wu, R. Girshick, P. Dollár, and C. Feichtenhofer, “Sam 2: Segment anything in images and videos,” 2024. [Online]. Available: <https://arxiv.org/abs/2408.00714>
- [35] B. Stellato, G. Banjac, P. Goulart, A. Bemporad, and S. Boyd, “Osqp: An operator splitting solver for quadratic programs,” *Mathematical Programming Computation*, vol. 12, no. 4, pp. 637–672, 2020.
- [36] K. Zakka, “Mink: Python inverse kinematics based on MuJoCo,” May 2025. [Online]. Available: <https://github.com/kevinzakka/mink>
- [37] Z. Bylinskii, T. Judd, A. Oliva, A. Torralba, and F. Durand, “What do different evaluation metrics tell us about saliency models?” *IEEE transactions on pattern analysis and machine intelligence*, vol. 41, no. 3, pp. 740–757, 2018.
- [38] W. Huang, C. Wang, Y. Li, R. Zhang, and L. Fei-Fei, “Rekep: Spatio-temporal reasoning of relational keypoint constraints for robotic manipulation,” in *Conference on Robot Learning*. PMLR, 2025, pp. 4573–4602.
- [39] A. Kirillov, E. Mintun, N. Ravi, H. Mao, C. Rolland, L. Gustafson, T. Xiao, S. Whitehead, A. C. Berg, W.-Y. Lo *et al.*, “Segment anything,” in *Proceedings of the IEEE/CVF international conference on computer vision*, 2023, pp. 4015–4026.

- [40] A. Radford, J. W. Kim, C. Hallacy, A. Ramesh, G. Goh, S. Agarwal, G. Sastry, A. Askell, P. Mishkin, J. Clark *et al.*, “Learning transferable visual models from natural language supervision,” in *International conference on machine learning*. PMLR, 2021, pp. 8748–8763.
- [41] M. Caron, H. Tovvron, I. Misra, H. Jégou, J. Mairal, P. Bojanowski, and A. Joulin, “Emerging properties in self-supervised vision transformers,” in *Proceedings of the IEEE/CVF international conference on computer vision*, 2021, pp. 9650–9660.
- [42] Y. Ze, G. Zhang, K. Zhang, C. Hu, M. Wang, and H. Xu, “3d diffusion policy: Generalizable visuomotor policy learning via simple 3d representations,” in *ICRA 2024 Workshop on 3D Visual Representations for Robot Manipulation*.
- [43] T. Gervet, Z. Xian, N. Gkanatsios, and K. Fragkiadaki, “Act3d: 3d feature field transformers for multi-task robotic manipulation,” in *7th Annual Conference on Robot Learning*, 2023. [Online]. Available: <https://openreview.net/forum?id=-HFJuX1uqs>